RSC Advances

PAPER

View Article Online
View Journal | View Issue

Cite this: *RSC Adv.*, 2019, **9**, 13543

Incorporating polyoxometalates and organic ligands to pursue 3d–4f heterometallic clusters: a series of $\{Cr_4Ln_4\}$ clusters stabilized by phthalic acid and $[SiW_{12}O_{40}]^{4-}$†

Ya-Nan Gu,[a] Dan Zhao,[b] Hao Yu,[a] Rui Ge,[a] Zhong Li,[a] Chong-Bian Tian,[c] Xin-Xiong Li,*[a] Yan-Qiong Sun[a] and Shou-Tian Zheng*[a]

Received 7th March 2019
Accepted 23rd April 2019

DOI: 10.1039/c9ra01731c

rsc.li/rsc-advances

By introduction of trilacunary Keggin-type polyoxometalate to the hydrothermal reaction system of Cr^{3+}, Ln^{3+} and phthalic acid, a series of novel $\{Cr_4Ln_4\}$ heterometallic clusters with the formula $Cs_2[Cr_4Ln_4(\mu_4\text{-}O)_4(\mu_3\text{-}O)_4(C_8H_4O_4)_4(H_2O)_{12}](H_3SiW_{12}O_{40})Cl\cdot 23H_2O$ (**1-Ln**, Ln = Ce, Pr, Nd) and $[Cr_4Ln_4(\mu_4\text{-}O)_4(\mu_3\text{-}O)_4(C_8H_4O_4)_4(H_2O)_{10}](H_6SiW_{12}O_{40})Cl_2\cdot 18H_2O$ (**2-Ln**, Ln = Sm, Eu, Gd, Tb, Dy, Ho, Er) have been obtained. Single-crystal structural analyses show that **1-Ln** and **2-Ln** constitute the first cases of Cr–Ln heterometallic clusters stabilized by inorganic polyoxometalate anions and organic ligands. Optical spectra studies demonstrate that **1-Ln** and **2-Ln** are narrow-gap semiconductors with band gaps of about 1.5 eV. Magnetic investigation shows that compound **2-Dy** is a potential single molecule magnet.

Introduction

The syntheses and investigation of unique 3d–4f heterometallic clusters have long been a field of great interest in modern inorganic chemistry.[1] The inherent contribution of the 3d and 4f electrons as well as the distinct magnetic couplings between two different metal ions within the heterometallic cluster often result in remarkable physicochemical, electronic, catalytic and magnetic properties, which makes 3d–4f heterometallic clusters promising functional materials to be used as single molecule magnets, molecular magnetic coolers, bifunctional catalysts and so on.[2] However, the preparation of 3d–4f heterometallic clusters is still not a simple task because of the various synthetic obstacles, such as different coordination number/geometries/affinity of 3d and 4f metal ions, charge matching and balance, and low yield caused by competing reactions between 3d and 4f metal ions with the same organic donor.[3] So far, most of reported works in this area focus on 3d–4f systems applying the later 3d transition metal including Fe^{3+}, Co^{2+}, Ni^{2+}, and Cu^{2+} ions mixed with lanthanide ions, resulting in several representative examples with intriguing structures and interesting properties.[4] In contrast, less efforts currently have been placed to employ the early transition metal ion Cr^{3+} to combine with lanthanide ions for constructing 3d–4f heterometallic clusters, probably due to the inert nature and rigid coordination characteristic of Cr^{3+} ion. The Cr^{3+} ion shows weaker anisotropy than those later transition metal ions such as Ni^{2+}, Co^{2+}.[5] Recent studies have also shown that the introduction of Cr^{3+} ion to combine with lanthanide ions with large anisotropy may generates new possibilities to obtain heterometallic Cr–Ln clusters with SMM behaviors.[6] This is because the weak Cr–Ln magnetic exchange interactions might strengthen the quantum tunneling of the magnetization, leading to the observation of the slow relaxation of the magnetization with a high energy barrier.[7] In this regard, the search of feasible approaches to design and construct new Cr–Ln heterometallic clusters is a highly desirable but challenging task.

Up to now, a few of Cr–Ln heterometallic clusters have been made by using Cr^{3+}, Ln^{3+} ions to react with specific organic chelating ligands. Typical examples include $\{CrLn_2\}$,[8] $\{Cr_2Ln_2\}$,[6b,7b] $\{Cr_2Ln_3\}$,[9] $\{Cr_4Ln\}$,[10] $\{Cr_2Ln_4\}$,[11] $\{Cr_3Ln_3\}$,[6b] $\{Cr_4Ln_4\}$,[6b,12] $\{Cr_3Ln_6\}$,[13] $\{Cr_6Ln_6\}$[5] and $\{Cr_8Ln_8\}$.[6a] Notably, the above Cr–Ln heterometallic clusters are all stabilized by only one type of organic ligand or simple inorganic oxo-anions such as sulfate radicals. It is believed that the introduction of a second ligand to the reaction system would bring new possibilities to achieve new Cr–Ln heterometallic clusters. In our exploration strategy, we are especially interested to introduce inorganic polyoxometalates (POMs) as a second ligand to cooperate with organic ligands for making new Cr–Ln

[a]State Key Laboratory of Photocatalysis on Energy and Environment, College of Chemistry, Fuzhou University, Fuzhou, Fujian 350108, China. E-mail: lxx@fzu.edu.cn; stzheng@fzu.edu.cn

[b]Fuqing Branch of Fujian Normal University, Fuqing, Fujian, 350300, China

[c]State Key Laboratory of Structural Chemistry, Fujian Institute of Research on the Structure of Matter, Chinese Academy of Sciences, Fuzhou, Fujian 350108, China

† Electronic supplementary information (ESI) available: Additional characterizations, additional tables, structural figures, and spectrum data. CCDC 1892101 and 1892102. For ESI and crystallographic data in CIF or other electronic format see DOI: 10.1039/c9ra01731c

heterometallic clusters, considering that anionic POM anions can serve as polydentate ligands, and transform into suitable configurations *in situ* to meet the coordination requirement in the final product.[14] Fortunately, in this contribution, Keggin-type polyanions have been successfully involved in the reaction system, and a series of novel Cr–Ln heterometallic clusters with general formula of $Cs_2[Cr_4Ln_4(\mu_4\text{-}O)_4(\mu_3\text{-}O)_4(C_8H_4O_4)_4(H_2O)_{12}](H_3SiW_{12}O_{40})Cl\cdot 23H_2O$ (**1-Ln**, Ln = Ce, Pr, Nd) and $[Cr_4Ln_4(\mu_4\text{-}O)_4(\mu_3\text{-}O)_4(C_8H_4O_4)_4(H_2O)_{10}](H_6SiW_{12}O_{40})Cl_2\cdot 18H_2O$ (**2-Ln**, Ln = Sm, Eu, Gd, Tb, Dy, Ho, Er) have been hydrothermally synthesized and fully characterized (Scheme 1). These compounds contain similar four-layered prismatic $[Cr_4Ln_4]$ cores, which to our knowledge constitute the first cases of Cr–Ln heterometallic clusters stabilized by both organic ligands and inorganic POM species.

Experimental section

Materials and measurements

$Na_{10}[\alpha\text{-}SiW_9O_{34}]\cdot 16H_2O$ was synthesized on the basis of literature method and proved by IR spectroscopy.[15] Other raw materials were analytical grade reagents, all of which were obtained from commercial sources and used without further purification. Infrared (IR) spectra (KBr particles) were tested on an Opus Vertex 70 FT-IR infrared spectrophotometer with a wavelength in the range of 500–4000 cm^{-1}. Elemental analyses of C, H were measured on a Vario EL Cube Germany Elementar. Powder X-ray diffraction (PXRD) patterns were tested on a Rigaku DMAX 2500 diffractometer with CuK_α radiation (λ = 1.54056 Å). Thermogravimetric analyses (TGA) were carried out on a DSC/DTA-TG Netzsch STA 449F5 analyzer under a nitrogen flow atmosphere with a heating rate of 10 °C min^{-1} at a temperature of 25–800 °C. The UV-Vis diffuse reflectance spectrum was carried out at UV-2600 Shimadzu Japan UV-Vis spectrophotometer ranging from 200 to 1200 nm with $BaSO_4$ as a reference. The PPMS-9T magnetometer with quantum design was used to measure the magnetization rate of polycrystalline samples at variable temperature within the range of 2–300 K under 0.1 tesla magnetic field. The experimental permittivity was modified to Pascal's constant. Ac impedance measurements were tested on zennium/IM6 impedance analyzer which the applied voltage was 50 mV and the frequency was in the scope of 0.1 Hz to 5 MHz. Constant temperature and humidity conditions were carried out by a STIK Corp. CIHI-150B incubator. The samples were pressed to form carbon-sample-carbon three layers of cylindrical sample (~3 mm thickness × 5 mm ϕ) coated with C-pressed electrodes. Two silver electrodes were attached to both sides of cylindrical sample to form four end terminals (quasi-four-probe method).

Synthesis of $Cs_2[Cr_4Ln_4(\mu_4\text{-}O)_4(\mu_3\text{-}O)_4(C_8H_4O_4)_4(H_2O)_{12}](H_3SiW_{12}O_{40})Cl\cdot 23H_2O$ (1-Ln, Ln = Ce, Pr, Nd). A mixture of $Na_{10}[\alpha\text{-}SiW_9O_{34}]\cdot 16H_2O$ (0.255 g, 0.093 mmol), $CrCl_3\cdot 6H_2O$ (0.102 g, 0.383 mmol), $Ln(NO_3)_3\cdot 6H_2O$ (0.461 mmol), phthalic acid (0.050 g, 0.301 mmol), Na_2CO_3 (0.051 g, 0.481 mmol), CsCl (0.053 g, 0.315 mmol), H_2O (5 mL) was adequately stirred for 1 h (pH_s = 3.8), and then was sealed in a 35 mL stainless steel reactor with a Teflon liner and kept at 140 °C. After 5 days, the reactor was cooled to room temperature naturally (pH_e = 3.2). Black block crystals were collected by filtration, washed with distilled water, and dried in air (Fig. S1†). Yield: *ca.* 43.0 mg (8.63% based on $Na_{10}[\alpha\text{-}SiW_9O_{34}]\cdot 16H_2O$). Elemental analysis calculated (%) for $C_{32}H_{89}O_{99}SiClCr_4Cs_2Ce_4W_{12}$ (Fw = 5361.86): C 7.16, H 1.67. Found (%): C 7.73, H 1.75. IR (KBr, cm^{-1}): 3346(s), 1570(vs), 1477(w), 1409(vs), 1386(w), 1172(w), 1007(w), 958(m), 910(vs), 783(s), 757(s), 690(m), 655(m), 577(w), 535(w).

Synthesis of $[Cr_4Ln_4(\mu_4\text{-}O)_4(\mu_3\text{-}O)_4(C_8H_4O_4)_4(H_2O)_{10}](H_6SiW_{12}O_{40})Cl_2\cdot 18H_2O$ (2-Ln, Ln = Sm, Eu, Gd, Tb, Dy, Ho, Er). **2-Ln** was prepared by a similar procedure in **1-Ln**. Keeping all reaction parameter the same as **1-Ln**, equal amount of heavy rare earth salts were used in the reactions (pH_s = 3.7, pH_e = 2.8). Black block crystals were collected by filtration, washed with distilled water, and dried in air (Fig. S1†). Yield: *ca.* 171 mg (36.21% based on $Na_{10}[\alpha\text{-}SiW_9O_{34}]\cdot 16H_2O$). Elemental analysis calculated (%) for $C_{32}H_{78}O_{92}SiCl_2Cr_4Tb_4W_{12}$ (Fw = 5083.66): C 7.56, H 1.54. Found (%): C 7.80, H 1.60. IR (KBr, cm^{-1}): 3324(m), 1560(vs), 1478(m), 1413(vs), 1386(w), 1173(w), 1007(w), 956(m), 910(vs), 788(s), 757(s), 689(m), 657(m), 586(s), 549(m).

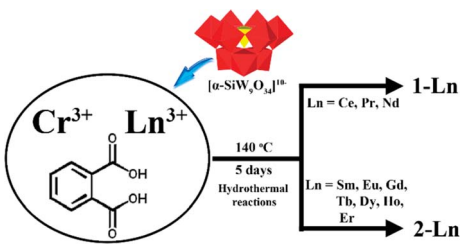

Scheme 1 The synthetic method for **1-Ln** and **2-Ln**.

Single-crystal structure analysis

Single crystals of **1-Ce** and **2-Tb** were selected as examples for crystal structure data collection. The crystallographic data of **1-Ce** and **2-Tb** were collected on a Bruker APEX2 duo CCD diffractometer under a nitrogen atmosphere (150 K) using graphite-monochromated Mo Kα radiation (λ = 0.71073). The direct method was used to solve the crystal structures, and the full-matrix least-squares refinement was performed based on F^2 according to the SHELX-2014 package. All non-hydrogen atoms were refined by using anisotropic thermal parameters. In **1-Ce** and **2-Tb**, the SiO_4 tetrahedra in Keggin-type $[SiW_{12}O_{40}]^{4-}$ polyanion were disordered into cubes, which is common in POM chemistry.[16] The determination of Cl^- anions in **1-Ce** and **2-Tb** was according to the results of SCXRD and EDS elemental mapping (Fig. S2–S3†). The identities of the other isostructural compounds were proved by single crystal indexing, PXRD characterizations and EDS spectra (Fig. S4†). The final formula of **1-Ce** and **2-Tb** were defined by combining the SCXRD results with C, H elemental analyses, TGA (Fig. S5†). An overview of the crystallographic data and structural refinements of **1-Ce** and **2-Tb** are summarized in Table 1. CCDC 1892101 (**1-Ce**) and 1892102 (**2-Tb**) comprise the supplementary crystallographic data for this paper.

Table 1 The X-ray crystallographic data for **1-Ce** and **2-Tb**[a]

	1-Ce	2-Tb
Empirical formula	$Cs_2Cr_4Ce_4O_{99}C_{32}$ $H_{89}Si_1W_{12}Cl_1$	$Cr_4Tb_4O_{92}C_{32}$ $H_{78}Si_1W_{12}Cl_2$
Formula weight	5361.87	5083.66
Crystal system	Triclinic	Triclinic
Space group	$P\bar{1}$	$P\bar{1}$
a (Å)	13.5174(11)	12.4544(9)
b (Å)	13.5216(11)	13.4312(9)
c (Å)	29.869(2)	31.842(2)
α (°)	81.6102(15)	80.2079(13)
β (°)	82.6279(16)	80.4562(12)
γ (°)	89.5941(17)	73.7358(12)
V (Å^3)	5356.0(8)	4999.4(6)
Z	2	2
F(000)	4466	4328
ρ_{calcd}	3.125	3.240
Temperature (K)	150(2)	150(2)
μ (mm^{-1})	15.682	17.117
Refl. Collected	41 293	37 382
Independent relf.	18 701	17 215
Parameters	1267	1240
GOF on F^2	1.091	1.066
Final R indices	$R_1 = 0.0658$	$R_1 = 0.0574$
($I = 2\sigma(I)$)	$wR_2 = 0.1818$	$wR_2 = 0.1463$
R indices (all data)	$R_1 = 0.0751$	$R_1 = 0.0676$
	$wR_2 = 0.1897$	$wR_2 = 0.1527$

[a] $R_1 = \sum||F_o| - |F_c||/\sum|F_o|$. $wR_2 = [\sum w(F_o^2 - F_c^2)^2/\sum w(F_o^2)^2]^{1/2}$; $w = 1/[\sigma^2(F_o^2) + (xP)^2 + yP]$, $P = (F_o^2 + 2F_c^2)/3$, where $x = 0.0897$, $y = 336.90$ for **1-Ce**; where $x = 0.0635$, $y = 302.83$ for **2-Tb**.

Results and discussion

Crystal structure description of 1-Ln and 2-Ln

In this contribution, compounds **1-Ce** and **2-Tb** were used as examples for the structural description. SCXRD analyses reveal that both **1-Ce** and **2-Tb** crystallize in monoclinic $P\bar{1}$ space group, and contain similar octanuclear heterometallic clusters, $[Cr_4Ce_4(\mu_4\text{-}O)_4(\mu_3\text{-}O)_4(\mu_2\text{-}O)_2(C_8H_4O_4)_4(H_2O)_{12}]$ (**Cr_4Ce_4**) and $[Cr_4Tb_4(\mu_4\text{-}O)_4(\mu_3\text{-}O)_4(\mu_2\text{-}O)_2(C_8H_4O_4)_4(H_2O)_{10}]$ (**Cr_4Tb_4**) (Fig. 1a and b), and identical Keggin-type $[SiW_{12}O_{40}]^{4-}$ polyanions (Fig. 1c). **Cr_4Ce_4** is consist of four Cr^{3+}, four Ce^{3+}, four μ_4-O atoms, four μ_3-O atoms, two μ_2-O and twelve water ligands. All Cr^{3+} ions adopt a regular octahedral geometry with two μ_4-O atoms, two μ_3-O atoms and two O atoms from two carboxylatic groups of two phthalic ligands. Each Ce^{3+} employs a nine-coordinated conformation. For Ce1 and Ce2, each of them is surrounded by two μ_3-O atoms, one μ_4-O atom, two carboxylate O atoms, one μ_2-H_2O (O3w/O17w) ligand and three terminal water molecules. While for Ce3 and Ce4, their coordination environments are similar with Ce1 and Ce2 except for the replacement of one terminal water ligand with one μ_2-O atom (O29/O28) from $[SiW_{12}O_{40}]^{4-}$ polyanion. The composition and structure of **Cr_4Tb_4** is similar with **Cr_4Ce_4** except for the removal of two μ_2-H_2O ligands. Additionally, all Tb^{3+} ions are eight-coordinated in **Cr_4Tb_4**. The oxidation states of Cr^{3+}, Ce^{3+} and Tb^{3+} are confirmed through bond valence sum calculations (Tables S1–S2†).[17] The deprotonated phthalic ligand exhibit a μ_4-η^1:η^1:η^1:η^1 coordination mode (Fig. 1d).[18] The Keggin-type $[SiW_{12}O_{40}]^{4-}$ polyanions were generated by *in situ* structural transformation from trilacuanry $[SiW_9O_{34}]^{10-}$ starting material, which is common in hydrothermal reactions.[19] In **Cr_4Ce_4**/**Cr_4Tb_4**, four Cr^{3+} ions are integrated by four μ_4-O atoms to form a cubane-like Cr_4O_4 cluster. Then, two dinuclear $[Ce_2(\mu_3\text{-}O)_2(H_2O)]$/$[Tb_2(\mu_3\text{-}O)_2]$ clusters cap on the top and bottom of the Cr_4O_4 cluster in a mutually perpendicular style, resulting in a four-layered heterometallic core $[Cr_4Ce_4(\mu_4\text{-}O)_4(\mu_3\text{-}O)_4(H_2O)_2]$/$[Cr_4Tb_4(\mu_4\text{-}O)_4(\mu_3\text{-}O)_4]$ (Fig. 1e and f). Such cores are much

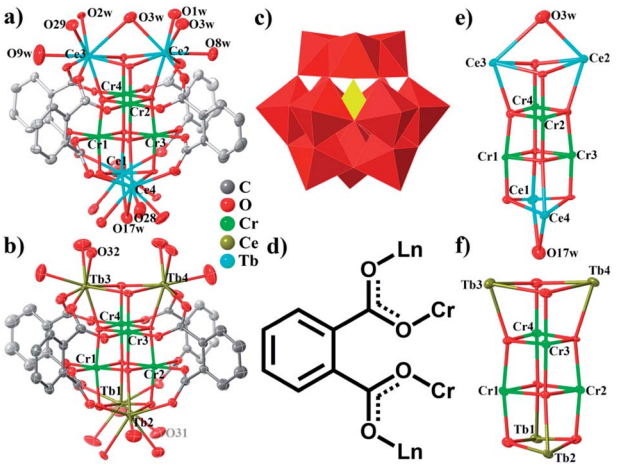

Fig. 1 (a) Structure of the $[Cr_4Ce_4(\mu_4\text{-}O)_4(\mu_3\text{-}O)_4(\mu_2\text{-}O)_2(C_8H_4O_4)_4(H_2O)_{12}]$ cluster; (b) structure of the $[Cr_4Tb_4(\mu_4\text{-}O)_4(\mu_3\text{-}O)_4(\mu_2\text{-}O)_2(C_8H_4O_4)_4(H_2O)_{10}]$ cluster; (c) structure of the Keggin-type $[SiW_{12}O_{40}]^{4-}$ polyanion; (d) view of the coordination mode of deprotonated phthalic ligand. In (a and b) and (e and f), the thermal ellipsoids were drawn at 50% level. Color codes: Ce, cyan; Tb, olive; Cr, green; W, blue; O red; C, gray; Si yellow. WO_6, red; SiO_4, yellow.

different from planar square-like $\{Cr_4Ln_4\}$ cores in Powell's work (Fig. S6†).[6b,12a] The four-layered cores are further stabilized by four deprotonated phthalic ligands, ten terminal water molecules and two μ_2-O atoms from two $[SiW_{12}O_{40}]^{4-}$ polyanions, giving rise to the neutral **Cr_4Ce_4/Cr_4Tb_4** clusters. The inter-connection between **Cr_4Ce_4/Cr_4Tb_4** clusters and $[SiW_{12}O_{40}]^{4-}$ polyanions further produces two kinds of 1-D zigzag cluster chains (Fig. 2). The difference between these chains is that half of $[SiW_{12}O_{40}]^{4-}$ polyanions exhibit different linking styles. Finally, the stacking of these cluster chains leads to the formation of 3-D structures which show irregular channels (Fig. S7–S8†).

It is noteworthy that Xu Yan and coworkers reported two heterometallic clusters containing similar four-layered $[Cr_4Ln_4(\mu_4\text{-}O)_4(\mu_3\text{-}O)_4]$ (Ln = Gd, Dy) cores very recently.[12b] However, **1-Ce** and **2-Tb** are much different from those in Xu Yan's work, mainly in the following areas: (1) the heterometallic cores in **1-Ce** and **2-Tb** are stabilized by both phthalic ligands and Keggin-type $[SiW_{12}O_{40}]^{4-}$ polyanions, while those in Xu Yan's work are only coordinated with isonicotinic ligands; (2) **1-Ce** and **2-Tb** are 1-D extended structures, whereas the compounds in Xu Yan's work are discrete clusters; (3) the rare earth ions in **1-Ce** and **2-Tb** can be replaced by other lanthanide ions (Pr^{3+}, Nd^{3+}, Sm^{3+}, Eu^{3+}, Gd^{3+}, Dy^{3+}, Ho^{3+}, Er^{3+}) to form another eight isologues, nonetheless, only Gd/Dy-based compounds were obtained in Xu Yan's work. In addition, a new methodology for clearly describing, classifying and searching high-nuclear clusters has been established and developed recently,[20–23] which consider each metal center as a node and every monatomic bridge as a linker. The resulting graph of each polynuclear compound can be described by a unique *NDk-m* symbol,[24] where *N* is the set of coordination numbers of topologically nonequivalent nodes, *D* is dimensionality; *D* = *M* for finite (molecular) clusters, *k* is the number of nodes in the cluster, and *m* enumerates topologically different clusters with the same *NDk* symbol. An isolated metal atom is designated (0). Thus, every *NDk-m* symbol denotes a topological type, *i.e.*, a set of topologically equivalent but likely conformationally different CC skeletons. Such method is also applicable to POM clusters, and has been successfully applied in compound like 4,4,5,6M52-1 for $[\{Co_4(OH)_3PO_4\}_4(A\text{-}\alpha\text{-}XW_9O_{34})_4]^{32-}$ (X = Si^{IV}, Ge^{IV}) and 3,6M16-1 for the central $\{Co_{16}\}$ unit.[25,26] In this context, compounds **1-Ce** and **2-Tb** can be described as a motif enumerated as 3,4,4,5,5M20-1 (Fig. S9†), and the 3d–4f heterometallic clusters unit can be described as 3,5M8-1 (Fig. S10†).

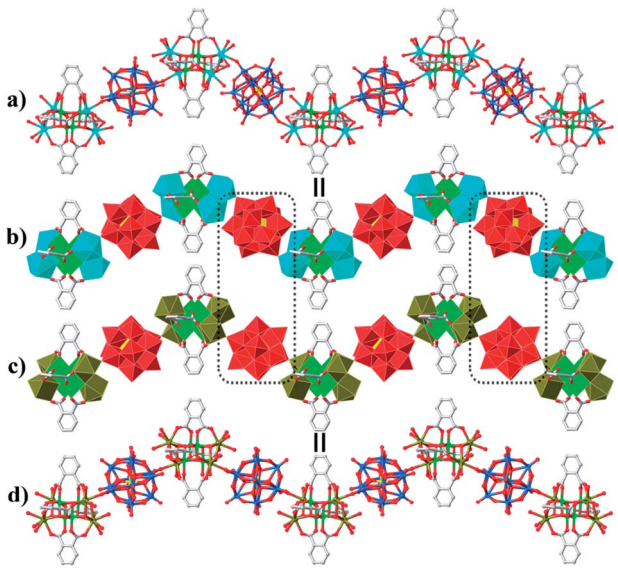

Fig. 2 (a and b) Polyhedral and stick representation of the 1-D heterometallic cluster chains in **1-Ce**. (c and d) Polyhedral and stick representation of the 1-D heterometallic cluster chains in **2-Tb**. Color codes: Ce, cyan; Tb, olive; Cr, green; W, blue; O red; C, gray; Si yellow; WO_6, red; SiO_4, yellow; CrO_6, green; CeO_9, cyan; TbO_8, olive.

Syntheses

Because of the inert characteristic, Cr^{3+} ion is not easy to combine with lanthanide ions to form high-nuclear heterometallic clusters. During the course of preparing **1-Ln** and **2-Ln**, we found that the following parameters have important influences on the crystal growth. First, Na_2CO_3 and CsCl are indispensible for making **1-Ln** and **2-Ln**. If anyone was removed from the reaction system, **1-Ln** and **2-Ln** cannot be obtained. Next, the optimal reaction temperature is about 140 °C. If the reactions were run at temperatures higher than 160 °C or lower than 120 °C, the yields decrease sharply. Additionally, we introduced other carboxylate ligands such as benzoic acid, isonicotinic acid, 4,5-imidazoledicarboxylic acid, to replace phthalic acid for further exploration. But, we were fruitless. What's more, we used different POMs precursors such as $[GeW_{11}O_{39}]^{8-}$, $[PW_9O_{34}]^{9-}$, $[GeW_9O_{34}]^{10-}$ to substitute $[\alpha\text{-}SiW_9O_{34}]^{10-}$ for further exploration. Unfortunately, we were failed to obtain suitable crystals. Finally, the radius of lanthanide ions show impact on the crystallization of the final structures. As well known, the radius of lanthanide ions are very close due to the presence lanthanide contraction. However, in our work, the lighter rare earth ions (Ce^{3+}, Pr^{3+}, Nd^{3+}) tend to form **1-Ln** series, whereas the heavier rare earth ions (Sm^{3+}, Eu^{3+}, Gd^{3+}, Tb^{3+}, Dy^{3+}, Ho^{3+}, Er^{3+}) prefer to crystallize in **2-Ln** series. These results indicate that the minor radius difference between rare earth ions still have obvious impact on the formation of the final products.

PXRD patterns, IR spectra, UV-Vis diffuse reflectance spectra

The good agreement between the experimental PXRD patterns and the calculated ones by Mercury software based on SCXRD results testifies that the as-prepared samples of **1-Ln** and **2-Ln** are pure phases (Fig. S11–S12†). In the IR spectra (Fig. S13–S14†), the peaks around 3359 cm^{-1} ascribe to the stretching vibration of –OH of the coordination water ligands. The vibration peaks located at 1400–1580 cm^{-1} correspond to the presence of the phenyl ring, carboxylate groups. The peaks at 957, 908, 879, 783 cm^{-1} attribute to the vibration of W–O_t, Si–O_c, W–O_b and W–O_c (O_t: terminal O atom; O_b: μ_2-O atom; O_c: μ_4-O atom), which attribute to characteristic vibrations of Keggin-type $[SiW_{12}O_{40}]^{4-}$ skeleton.[27] In addition, the adsorption peaks in the range of 780–600 cm^{-1} derive from the stretching

vibrations of the Cr–O[28] and Ln–O[12b] bonds in the heterometallic cluster. The ultraviolet-visible diffuse reflectance spectra with $BaSO_4$ as reference were also measured to evaluate the light-harvesting properties of **1-Ce** and **2-Tb** (Fig. S15†). It can be seen from the spectra that the two crystals have obvious absorption in the visible-ultraviolet region. The band gap energies were 1.49 eV for **1-Ce** and 1.50 eV for **2-Tb** according the fitting curve of Kubelka–Munk Function[29] *vs.* energy (eV), indicating the potential applications of compounds **1-Ce** and **2-Tb** as semiconductor materials.

Magnetic properties

Considering the presence of large unquenched orbital angular momentum in Tb^{3+} and Dy^{3+}, **2-Tb** and **2-Dy** were selected for magnetic studies. The temperature-dependent magnetic susceptibility of **2-Tb** and **2-Dy** were measured at the temperature range of 2 to 300 K with the applied magnetic field of 1 kOe. As shown in Fig. 3a and b, the experimental $\chi_m T$ values of **2-Tb**/**2-Dy** are 54.95/66.61 cm^3 K mol^{-1} at room temperature, which are conforming to the theoretical values of 50.80/61.59 cm^3 K mol^{-1} based on four non-interacting Cr^{3+} ($S = 3/2$ and $g = 2$) ions and four isolated Tb^{3+} ($^7F_6$, $S = 3$, $L = 3$, $g = 3/2$, $C = 11.82$ cm^3 K mol^{-1})/Dy^{3+} ($^6H_{15/2}$, $S = 5/2$, $L = 5$, $g = 4/3$, $C = 14.17$ cm^3 K mol^{-1}) ions. In **2-Tb**, the experimental $\chi_m T$ value decreases slowly from 54.95 to 51.54 cm^3 K mol^{-1} along with the temperature decreasing from 300 to 36 K, and then falls sharply to 21.47 cm^3 K mol^{-1} at 2 K. The continuous downward behaviour demonstrates the existence of overall antiferromagnetic interactions with **2-Tb**. Such result is consistent with that in Xu Yan's work.[12b] In **2-Dy**, upon cooling, the $\chi_m T$ value increases to a maximum of 91.05 cm^3 K mol^{-1} at 28 K. Upon cooling below 28 K, the $\chi_m T$ value decreases sharply to reach to the minimum value of 32.16 cm^3 K mol^{-1} at 2 K. Such a behaviour suggests the coexistence of both ferromagnetic and antiferromagnetic interactions between metal centers in **2-Dy**. The fittings of $1/\chi_m$ *vs* T curves found that **2-Tb**/**2-Dy** abide the Curie–Weiss rule in the range of 2–300/50–300 K, respectively, giving Curie constants and Weiss constants of 54.56 cm^3 mol^{-1} and −3.07 K for **2-Tb**, and 62.58 cm^3 mol^{-1} and 14.97 K for **2-Dy**. The negative Weiss constant further support the occurrence of antiferromagnetic interactions within **2-Tb**, while the positive Weiss constant proves the presence of main ferromagnetic interactions in **2-Dy**.

A more detailed analyses of the field-dependent isothermal magnetization behaviors of **2-Tb**/**2-Dy** were carried out under 0–80 kOe at 2 K (Fig. 3c and d). In **2-Tb**, the M value rises rapidly to 24.21 Nβ at 28 kOe, then it grows steady to the maximum value of 26.87 Nβ at 80 kOe, which much lower than the theoretical value of 36 Nβ according to four non-interacting Tb^{3+} and four Cr^{3+} ions. Such deviation illustrates the presence of a significant magnetic anisotropy and/or low lying excited states.[5] In **2-Dy**, the M value shows a similar trend in **2-Tb**. the maximum value of 37.97 Nβ occur at 80 kOe, is in good agreement of theoretical value of 32 Nβ according to four non-interaction Dy^{3+} and four Cr^{3+}. Such a saturation in magnetization is also found in previous works.[11b]

In order to investigate whether the magnetic interaction between metal ions can cause the properties of single molecule magnets, the variable-temperature alternating current susceptibility of **2-Tb** and **2-Dy** at frequencies from 111 to 2311 Hz in the scope of 2–20 K were tested (Fig. 4). The in-phase (χ') and out-of-phase (χ'') plots of **2-Tb** do not exhibit obvious frequency-dependent behaviours. Nevertheless, the in-phase (χ') and out-of-phase (χ'') values of **2-Dy** shows weak frequency dependent, which indicates the potential single molecule magnetic behaviour. Such a slow relaxation might arise from the anisotropic Dy^{3+} ions associated with its relatively large ground spin states.[11b] There is no maximum in χ'', which may be caused by fast quantum tunnelling effect.[30]

Proton conduction properties

Proton-conductive materials are an important class of promising materials in the fuel cells and battery preparation.[31] Considering that there are a lot of lattice water molecules, and

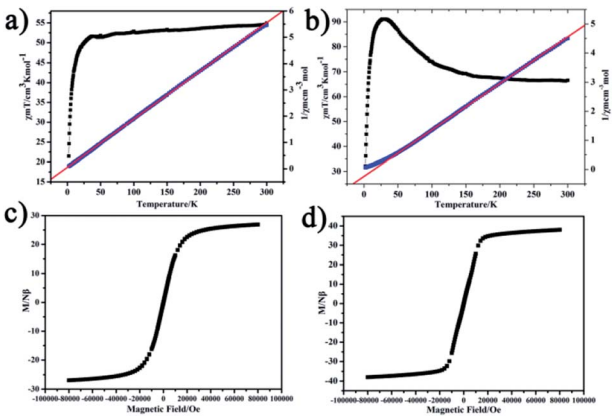

Fig. 3 (a and b) The temperature-dependent $\chi_m T$ (black) and $1/\chi_m$ (blue) curves of **2-Tb** (a) and **2-Dy** (b) in the applied magnetic field of 1 kOe with the temperature range of 2–300 K. The red lines are the fitting of $1/\chi_m$ *versus* T curves according to the Curie–Weiss rule. (c and d) Field variation of magnetic susceptibility in 2 K for **2-Tb** (c) and **2-Dy** (d).

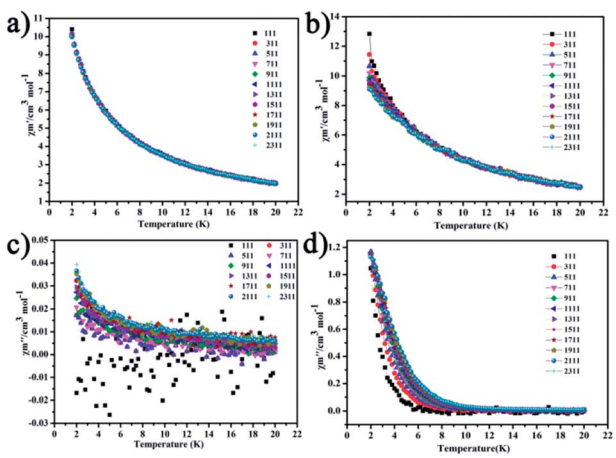

Fig. 4 Frequency-dependent behavior of χ'_m and χ''_m for **2-Tb** (a and c) and **2-Dy** (b and d) in zero static field at 2–20 K.

the good water stability of **1-Ln** and **2-Ln**, we selected **1-Ce** and **2-Tb** as examples to evaluate their proton conductive ability. The proton conductivities were measured by using compacted granular crystalline powder samples, AC impedance measurements and evaluated from the half-circles in the Nyquist plots. By using the equivalent circuit simulation of the ZSimpWin software, the resistance value is extrapolated from the impedance data. The following equation was used to calculate the conductivity: $\sigma = L/RS$, where σ is the conductivity, L is the thickness (~0.160 cm for **1-Ce**; ~0.178 cm for **2-Tb**) and S is the cross section of the particle (0.5 cm ϕ). The volume resistance R is extracted directly from the impedance graph. Firstly, the conductivities were measured on relative humidity (RH) with 55%, 70%, 85%, 98% RH respectively at a constant temperature of 30 °C for **1-Ce** and **2-Tb**. As shown in Fig. 5a 6a, the conductivities of **1-Ce** and **2-Tb** at 30 °C with 55% RH are 1.04×10^{-6} S cm^{-1} and 1.17×10^{-6} S cm^{-1}, respectively. When the RH increases from 55% to 98%, the conductivities increase to 1.16×10^{-5} S cm^{-1} and 1.80×10^{-5} S cm^{-1} for **1-Ce** and **2-Tb**, respectively. The enhanced conductivities should be ascribed to that more water molecules entered into the crystal lattice. Furthermore, the conductivities were tested at temperature of 30 °C, 40 °C, 50 °C, 60 °C, 70 °C, 80 °C with constant RH of 98% for **1-Ce** and **2-Tb** (Fig. 5b and c, 6b and c). When the temperatures increased from 30 °C to 80 °C, the conductivities of **1-Ce** and **2-Tb** enhanced from 1.16×10^{-5} S cm^{-1} to 8.72×10^{-4} S cm^{-1} and from 1.80×10^{-5} S cm^{-1} to 2.37×10^{-3} S cm^{-1}, separately. These values are comparable to most proton-conducting metal–organic framework materials[32] and some POM-based materials.[33] The enhancement of conductivities should be attributed to that the ion transition rates in the crystal lattice were accelerated as the temperatures increased.[34] Meanwhile, these values also indicate that temperatures exhibit more important impact on conductivities than RH. Finally, according to the Arrhenius equation $\sigma T = \sigma_0 \exp(-E_a/k_b T)$, the activation energies E_a at 98% RH were estimated to be 0.81 and 0.94 eV for **1-Ce** and **2-Tb** (Fig. 5d, 6d), respectively. The mechanism of ion conduction is that vehicular mechanism

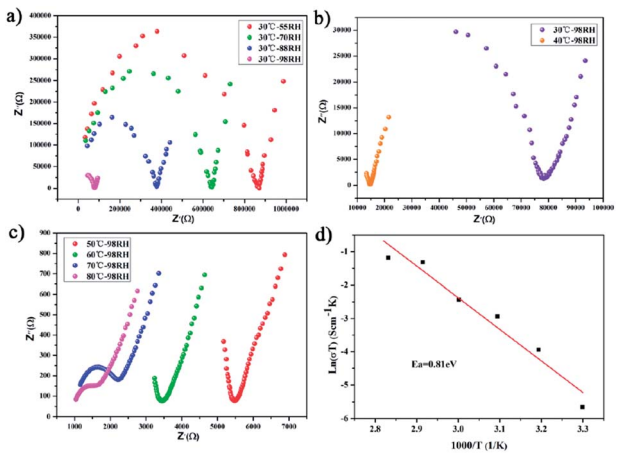

Fig. 5 (a) Nyquist plots for **1-Ce** at different RHs and $T = 30$ °C; (b and c) Nyquist plots for **1-Ce** at different temperatures and 98% RH; (d) Arrhenius plots of the conductivity of **1-Ce**.

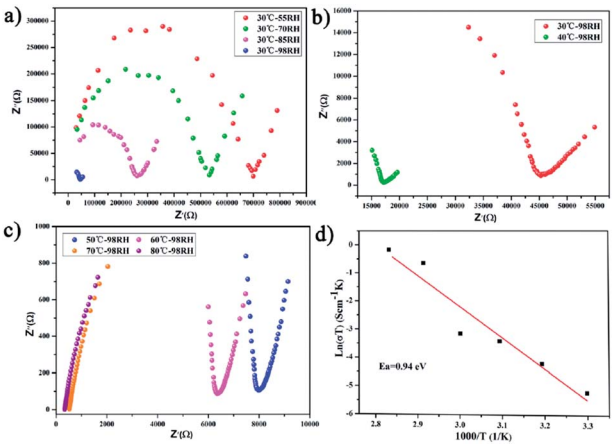

Fig. 6 (a) Nyquist plots for **2-Tb** at different RHs and $T = 30$ °C; (b and c) Nyquist plots for **2-Tb** at different temperatures and 98% RH; (d) Arrhenius plots of the conductivity of **2-Tb**.

plays a leading role, on account of the activation energies greater than 0.4 eV, which is expounded that there are ion conduction channels in the structure, and ions conduct electricity in the structure by means of transportation.[35] The proton conduction in our materials is mainly carried out through hydrogen-bonding network among water molecules and protons, which is resulted from a combination of POMs, 3d–4f heterometalic clusters and organic species.[36,37]

Conclusions

A family of octanuclear 3d–4f heterometallic clusters, **1-Ln** and **2-Ln**, have been hydrothermally made. SCXRD structural analyses reveal that all compounds are constructed from novel $\mathbf{Cr_4Ln_4}$ cores stabilized by phthalic ligands and Keggin-type POMs. Optical spectra studies demonstrate that these materials are narrow-gap semiconductors with band gaps of about 1.5 eV. The magnetic investigation reveals the presence of antiferromagnetic interactions within the $\mathbf{Cr_4Tb_4}$ core and the coexistence of ferromagnetic and antiferromagnetic couplings with $\mathbf{Cr_4Dy_4}$ core. What's more, **2-Dy** shows a single molecule magnet behaviour. Finally, proton conductive measurements reveal that **1-Ce** and **2-Tb** exhibit moderate conductivities at 80 °C with 98% RH. Our results also prove that the introduction of POM clusters to combine with organic chelating ligands as structure directing agents is an effective route to pursue unique 3d–4f heterometallic clusters. Further work focused on pursuing higher-nuclear Cr–Ln heterometallic clusters is underway in our group.

Conflicts of interest

The authors declare no competing financial interest.

Acknowledgements

This work was financially supported by National Natural Science Foundation of China (No. 21671040 and 21773029) and

the Natural Science Foundation of Fujian Province (No. 2017J01579).

Notes and references

1 (*a*) K. Griffiths and G. E. Kostakis, *Dalton Trans.*, 2018, **47**, 12011; (*b*) S. Fan, S. H. Xu, X. Y. Zheng, Z. H. Yan, X. J. Kong, L. S. Long and L. S. Zheng, *CrystEngComm*, 2018, **20**, 2120; (*c*) J. W. Zhao, Y. Z. Li, L. J. Chen and G. Y. Yang, *Chem. Commun.*, 2016, **52**, 4418.

2 (*a*) D. P. Liu, X. P. Lin, H. Zhang, X. Y. Zheng, G. L. Zhuang, X. J. Kong, L. S. Long and L. S. Zheng, *Angew. Chem., Int. Ed.*, 2016, **55**, 4532; (*b*) Y. N. Gu, Y. Chen, Y. L. Wu, S. T. Zheng and X. X. Li, *Inorg. Chem.*, 2018, **57**, 2472; (*c*) S. K. Singh, M. F. Beg and G. Rajaraman, *Chem.–Eur. J.*, 2016, **22**, 672; (*d*) L. Jiang, B. Liu, H. W. Zhao, J. L. Tian, X. Liu and S. P. Yan, *CrystEngComm*, 2017, **19**, 1816.

3 (*a*) Y. N. Gu, H. Yu, L. D. Lin, Y. L. Wu, Z. Li, W. Y. Pan, J. He, L. Chen, Q. Li and X. X. Li, *New J. Chem.*, 2019, **43**, 3011; (*b*) Q. Lin, Y. Zhang, W. Cheng, Y. Liu and Y. Xu, *Dalton Trans.*, 2017, **46**, 643.

4 (*a*) S. Chen, V. Mereacre, C. E. Anson and A. K. Powell, *Dalton Trans.*, 2016, **45**, 98; (*b*) K. R. Vignesh, S. K. Langley, K. S. Murray and G. Rajaraman, *Chem.–Eur. J.*, 2017, **23**, 1654; (*c*) X. Y. Zheng, X. J. Kong, Z. Zheng, L. S. Long and L. S. Zheng, *Acc. Chem. Res.*, 2018, **51**, 517.

5 S. Chen, V. Mereacre, Z. Zhao, W. Zhang, M. Zhang and Z. He, *Dalton Trans.*, 2018, **47**, 7456.

6 (*a*) L. Qin, J. Singleton, W. P. Chen, H. Nojiri, L. Engelhardt, R. E. P. Winpenny and Y. Z. Zheng, *Angew. Chem., Int. Ed.*, 2017, **56**, 16571; (*b*) J. Rinck, Y. Lan, C. E. Anson and A. K. Powell, *Inorg. Chem.*, 2015, **54**, 3107.

7 (*a*) S. Chen, V. Mereacre, C. E. Anson and A. K. Powell, *Dalton Trans.*, 2016, **45**, 9336; (*b*) S. K. Langley, D. P. Wielechowski, B. Moubaraki and K. S. Murray, *Chem. Commun.*, 2016, **52**, 10976.

8 P. E. Car, A. Favre, A. Caneschi and R. Sessoli, *Dalton Trans.*, 2015, **44**, 15769.

9 X. Q. Wang, Z. Y. Li, Z. X. Zhu, J. Zhu, S. Q. Liu, J. Ni and J. J. Zhang, *Eur. J. Inorg. Chem.*, 2013, 5153.

10 O. Blacque, A. Amjad, A. Caneschi, L. Sorace and P. E. Car, *New J. Chem.*, 2016, **40**, 3571.

11 (*a*) H. Xiang, W. G. Lu, W. X. Zhang and L. Jiang, *Dalton Trans.*, 2013, **42**, 867; (*b*) H. Xiang, W. G. Lu, L. Jiang, W. X. Zhang and Y. Lan, *Eur. J. Inorg. Chem.*, 2016, **6**, 907.

12 (*a*) J. Rinck, G. Novitchi, W. Van den Heuvel, L. Ungur, Y. Lan, W. Wernsdorfer, C. E. Anson, L. F. Chibotaru and A. K. Powell, *Angew. Chem., Int. Ed.*, 2010, **49**, 7583; (*b*) C. Cui, J. P. Cao, X. M. Luo, Q. F. Lin and Y. Xu, *Chem.–Eur. J.*, 2018, **24**, 15295; (*c*) M. Perfetti1, J. Rinck, G. Cucinotta, C. E. Anson, X. Gong, L. Ungur, L. Chibotaru, M.-E. Boulon1, A. K. Powell and R. Sessoli1, *Front. Chem.*, 2019, **7**, 6.

13 S. Schmitz, J. van Leusen, N. V. Izarova, Y. Lan, W. Wernsdorfer, P. Kögerler and K. Y. Monakhov, *Dalton Trans.*, 2016, **45**, 16148.

14 (*a*) S. T. Zheng and G. Y. Yang, *Chem. Soc. Rev.*, 2012, **41**, 7623; (*b*) X. X. Li, Y. X. Wang, R. H. Wang, C. Y. Cui, C. B. Tian and G. Y. Yang, *Angew. Chem., Int. Ed.*, 2016, **55**, 6462.

15 A. P. Ginsberg, *Inorg. Synth.*, 1990, **27**, 87.

16 (*a*) J. X. Lin, J. Lü, H. X. Yang and R. Cao, *Cryst. Growth Des.*, 2010, **10**, 1966; (*b*) X. X. Li, L. Chen, W. H. Fang and G. Y. Yang, *Acta Chim. Sin.*, 2013, **71**, 179.

17 I. D. Brown and D. Altermatt, *Acta Crystallogr., Sect. B: Struct. Sci.*, 1985, **41**, 244.

18 X. Li and R. Cao, *J. Solid State Chem.*, 2012, **196**, 182.

19 (*a*) Y. W. Li, L. Y. Guo, H. F. Su, M. Jagodič, M. Luo, X. Q. Zhou, S. Y. Zeng, C. H. Tung, D. Sun and L. S. Zheng, *Inorg. Chem.*, 2017, **56**, 2481; (*b*) Y. Ghandour, A. B. Khelifa, M. S. Belkhiria, C. Daiguebonne, S. Freslon, O. Guillou and T. Roisnel, *Polyhedron*, 2016, **115**, 1.

20 G. E. Kostakis and A. K. Powell, *Coord. Chem. Rev.*, 2009, **253**, 2686.

21 G. E. Kostakis, V. A. Blatov and D. M. Proseprio, *Dalton Trans.*, 2012, **41**, 4634.

22 C. Wu, S. Datta, W. Wernsdorfer, G. H. Lee, S. Hill and E. C. Yang, *Dalton Trans.*, 2010, **39**, 10160.

23 V. A. Grillo, Z. Sun, K. Folting, D. N. Hendrickson and G. Christou, *Chem. Commun.*, 1996, 2233.

24 E. V. Alexandrov, V. A. Blatov, A. V. Kochetkov and D. M. Proserpio, *CrystEngComm*, 2011, **13**, 3947.

25 M. Ibrahim, A. Haider, Y. Xiang, B. S. Bassil, A. M. Carey, L. Rullik, G. B. Jameson, F. Doungmene, I. M. Mbomekallė, P. de Oliveira, V. Mereacre, G. E. Kostakis, A. K. Powell and U. Kortz, *Inorg. Chem.*, 2015, **54**, 6136.

26 M. Ibrahim, A. Haider, Y. Lan, B. S. Bassil, A. M. Carey, R. Liu, G. Zhang, B. Keita, W. Li, G. E. Kostakis, A. K. Powell and U. Kortz, *Inorg. Chem.*, 2014, **53**, 5179.

27 (*a*) R. Thouvenot, M. Fournier, R. Franck and C. Rocchiccioli-Deltcheff, *Inorg. Chem.*, 1984, **23**, 598; (*b*) T. Yang, X. X. Li and S. T. Zheng, *Chin. J. Struct. Chem.*, 2017, **36**, 1729.

28 X. Li, H. Xu, F. Kong and R. Wang, *Angew. Chem., Int. Ed.*, 2013, **52**, 13769.

29 V. M. Huxter, T. Mirkovic, P. S. Nair and G. D. Scholes, *Adv. Mater.*, 2008, **20**, 2439.

30 S. Y. Lin, G. F. Xu, L. Zhao, Y. N. Guo, Y. Guo and J. Tang, *Dalton Trans.*, 2011, **40**, 8213.

31 B. Gil-Hernández, S. Savvin, G. Makhloufi, P. Núñez, C. Janiak and J. Sanchiz, *Inorg. Chem.*, 2015, **54**, 1597.

32 W. H. Fang, L. Zhang, J. Zhang and G. Y. Yang, *Chem.–Eur. J.*, 2016, **22**, 2611.

33 Z. Li, X. X. Li, T. Yang, Z. W. Cai and S. T. Zheng, *Angew. Chem., Int. Ed.*, 2017, **129**, 2708.

34 Z. Li, X. X. Li and S. T. Zheng, *Inorg. Chem. Commun.*, 2017, **80**, 27.

35 K. D. Kreuer, A. Rabenau and W. Weppner, *Angew. Chem., Int. Ed.*, 1982, **21**, 208.

36 Z. Li, L. D. Lin, H. Yu, X. X. Li and S. T. Zheng, *Angew. Chem., Int. Ed.*, 2018, **57**, 15777.

37 K. Niinomi, S. Miyazawa, M. Hibino, N. Mizuno and S. Uchida, *Inorg. Chem.*, 2017, **56**, 15187.